ACS OMEGA

http://pubs.acs.org/journal/acsodf

Article

Hydroxylated Graphene: A Promising Reinforcing Nanofiller for Nanoengineered Cement Composites

Sen Yang, Wen Jia, Yuangui Wang, Weifu Zhang, and Xiaoya Yuan*

Cite This: *ACS Omega* 2021, 6, 30465−30477

Read Online

ACCESS | Metrics & More | Article Recommendations | Supporting Information

ABSTRACT: A very low dosage of graphene oxide (GO) can enhance the mechanical durability of cement composites, but the reinforcing enhancement is highly dependent on the uniform dispersion of graphene in the matrix. Carboxylic groups at GO nanosheets have a decisive effect on GO aggregation in an alkaline cement solution because they have a strong complexation ability with aqueous Ca^{2+} released by cement hydration and subsequently crosslinks the adjacent graphene sheets, causing the immediate coagulation of GO. The available methods of homogeneously dispersing GO in a cement slurry cannot completely eliminate this carboxylic-crosslinking-induced GO coagulation. In this study, many hydroxyl groups were introduced onto the edge and planar nanosheets to prepare water-soluble hydroxylated graphene (HO-G) by facile ball milling. The structure of HO-G was thoroughly characterized in detail, and its dispersion behavior in pure water and $Ca(OH)_2$ was extensively investigated. These results showed that the prepared HO-G exhibited good hydrophilicity and excellent colloidal dispersion ability against high pH and Ca^{2+} ions compared to GO. The effect of HO-G on the workability, mechanical strength, and chloride penetrability of a cement mortar was further studied. At a content of 0.03% by cement mass, HO-G provided 28.62 and 21.19% enhancements of compressive strength and 3.85 and 7.89% enhancements of flexural strength at 3 and 28 days, respectively, while the non-steady-state migration coefficient decreased by 31.51% compared to the reference mortar. Compared to GO, a lower dosage of HO-G exhibited a similar reinforcing effect to cement composites with little adverse impact on the fluidity of the fresh cement slurry. Moreover, the addition of HO-G could refine the pore structure, accelerate the hydration process of cement to some degree, and generate more hydration products so that the structure of the cement mortar was densified. Considering its environmentally friendly preparation, HO-G, as a promising reinforcing nanofiller, could provide a new solution to develop nanoengineered cement composites.

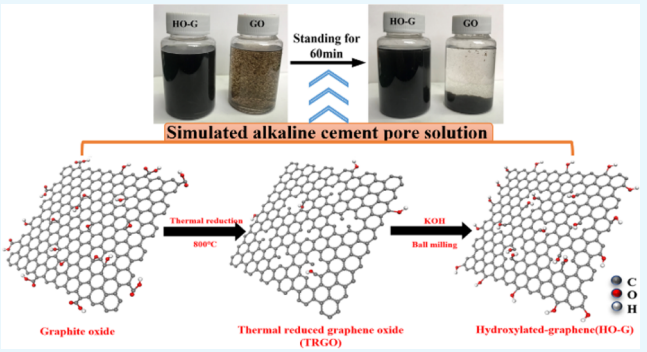

1. INTRODUCTION

Graphene-based nanosheets have been widely studied due to their reinforcement and functionalization of cementitious composites in recent years. As novel two-dimensional (2D) carbon nanomaterials, a number of studies have reported that the incorporation of an appropriate amount of graphene and its derivatives into cement composites can remarkably enhance their mechanical properties, durability, and conductivity.[1,2] Nevertheless, due to the unique structure of graphene, there are strong van der Waals force and $\pi-\pi$ stacking between the adjacent layers,[2] and at the same time, it has a large specific surface area, which leads to its easy agglomeration and causes difficulty in dispersing uniformly in an aqueous solution.[3] As a derivative of 2D graphene nanosheets, the layered structure of graphene oxide (GO) is similar to that of graphene, and the oxygen-containing functional groups, including hydroxyl, epoxy, and carboxylic groups, render GO hydrophilic;[4] thus, GO was intensively studied as a nanoreinforcing filler in nanoengineered cement composites.[5] However, the excellent water solubility of GO does not guarantee homogenous dispersion in cement alkaline solution. Several studies reported that both the pH value and cation valence played an important role in the GO colloidal solution in the aquatic environment.[6,7] Chowdhury et al.[8] investigated the aggregation, adsorption, and morphological transformation of GO in the presence of common environmental cations and indicated that divalent cations such as Ca^{2+} and Mg^{2+} could induce GO aggregation. Gao et al.[9] reported that pH also influenced the stability of GO. Severe coagulation of GO was observed in both the cement pore solution[10] and the cement paste.[11] Ghazizadeh et al.[12] investigated the colloidal stability of GO in the alite paste environment and indicated that GO was easy to coagulate in

Received: July 20, 2021
Accepted: October 22, 2021
Published: November 1, 2021

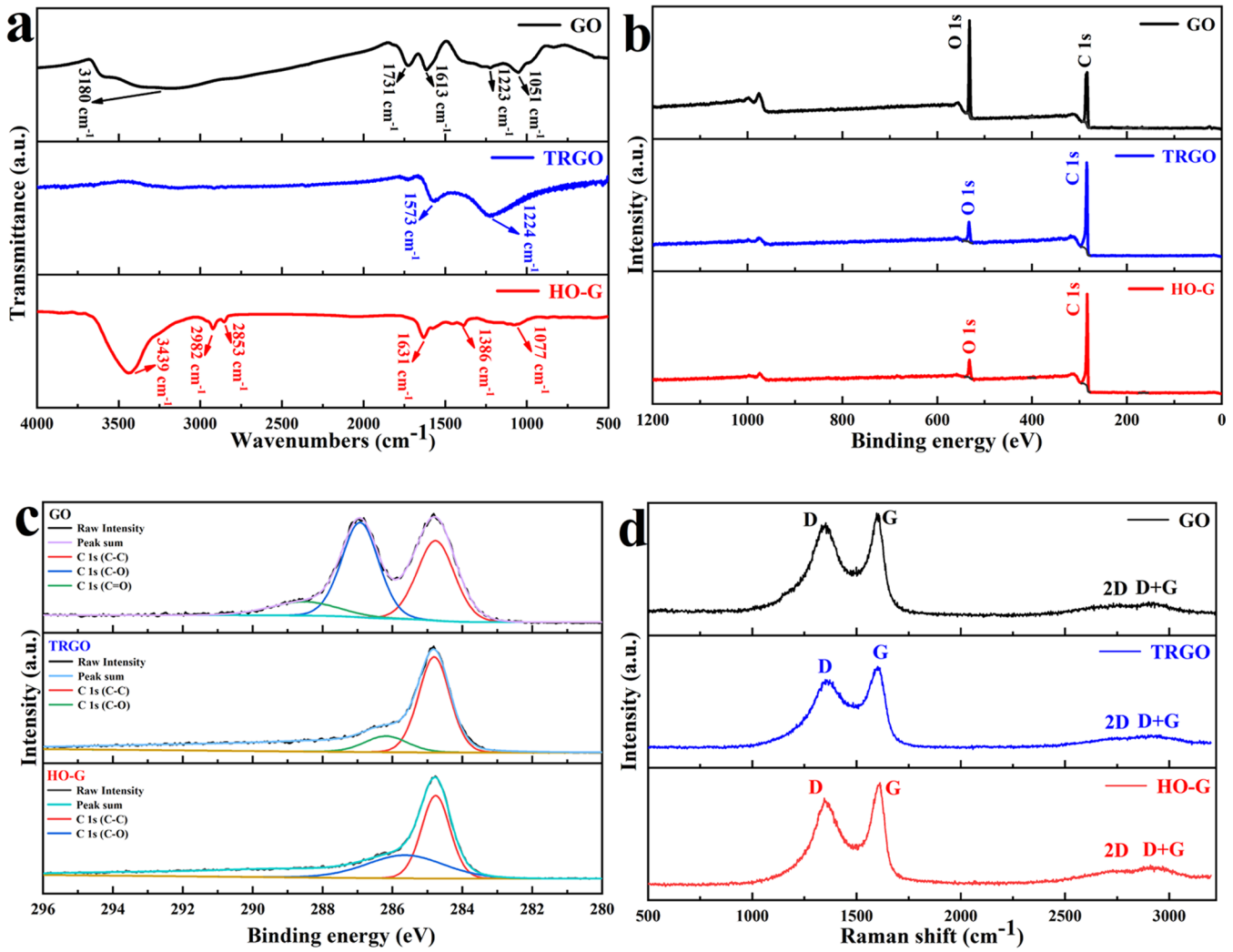

Figure 1. (a) FTIR spectra, (b) XPS survey and (c) high-resolution XPS C 1s spectra, (d) Raman spectra of GO, TRGO, and HO-G.

the alite paste. The instability of GO dispersion in the cement pore solution is due to (i) the cross-linking between GO by Ca^{2+} or hydration crystals through "bridging" the carboxyl groups at the edges of GO sheets[13,14] and (ii) the reduction of partially functional groups in GO at high pH.[15] The formation of large GO sediments by aggregation not only hampered its homogeneous dispersion in the cement matrix[16] but also reduced the fluidity of the cement slurry.[17] Shang et al.[18] reported that the minislump diameter of the cement paste decreased by 36.2% when 0.08 wt % GO by the cement weight was added. Good fluidity is a guarantee of mechanical properties and workability of cement composites, which is extremely essential for cement engineering applications.[19] Consequently, the uniform dispersion of GO in the cement hydration medium plays a vital role in enhancing the cement composites.

Various physical and chemical techniques have been performed to improve the dispersion of GO in the cement matrix, including mechanical ultrasonication, the usage of surfactants, and chemical functionalization.[5,16] Ultrasonic dispersion is the most common technique used to achieve the dispersion of nanosheets before adding nanomaterials to cement.[20] Chemical functionalization is mainly to graft functional groups to the surface of GO through the covalent linkage.[21] Several researchers also use surfactants, which can be adsorbed onto the GO surface and reduce surface energy, improving the dispersion of GO in cement composites.[22] Nonetheless, none of the existing methods can avoid the cross-linking between the carboxyl groups of GO nanosheets and Ca^{2+} released from cement hydration. In other words, more or less aggregation of GO in the cement hydration medium cannot be completely avoided by employing these available methods so that the remarkable reinforcement of GO to cement composites cannot be fully exerted.

Upon deep insight into the coagulation of GO, whether in water or cement pore solution, the carboxylated group on the edges of nanosheets has a dominant influence on the dispersion stability of the GO solution. Presumably, reducing the content of −COOH can improve the stability of GO in the alkaline cement pore solution while decreasing the water solubility of graphene. Keeping in mind the prerequisite that graphene must be functionalized to be hydrophilic, a new graphene derivative can be prepared by grafting more hydroxyl groups onto the planar sheet when decreasing the content of the carboxylic group. In our study, to increase the content of hydroxyl groups on the basal plane of graphene, porous thermally reduced graphene oxide (TRGO) was employed as the raw material to prepare hydroxylated graphene (HO-G) using one-step solid-state ball milling. Hydroxyl groups were distributed on the edges of both planar sheets and inner

https://doi.org/10.1021/acsomega.1c03844
ACS Omega 2021, 6, 30465−30477

nanopores. Compared to the time-consuming GO preparation method where flammable and explosive chemicals (e.g., H_2SO_4, $KMnO_4$) are commonly used,[23,24] the synthesis of HO-G is facile and environmentally friendly. Despite the fact that HO-G has previously been reported to be biocompatible[25,26] and electroactive[27] materials, no study reported the use of HO-G as a reinforcing nanofiller in cementitious composites.

In this paper, the structure of HO-G was fully characterized and its dispersion stability was elaborately compared to that of GO in deionized (DI) water, aqueous $CaCl_2$ solution, and saturated $Ca(OH)_2$ solution, respectively. Furthermore, the effect of HO-G on the workability, mechanical strength, and chloride penetrability of cement mortars was investigated. Finally, the effect of HO-G on the hydration degree and pore structure of cement composites was characterized by a nonevaporative water (NEW) content, an X-ray diffraction (XRD) pattern, mercury intrusion porosimetry (MIP), and scanning electron microscopy (SEM). These disclosed results showed that HO-G exhibited an excellent dispersion ability in a simulated cement pore solution, and as one of the nanomaterials, it could be a promising reinforcing nanofiller and hold the potential to provide a breakthrough in nanoengineered cement composites.

2. RESULTS AND DISCUSSION

2.1. Structural Characterization of HO-G. Water-soluble hydroxylated graphene (HO-G) was reported in previous studies.[25−27] Dai et al.[26] used solid KOH powder and graphite flakes to prepare HO-G by ball milling, in which graphite layers were peeled off under the violent action of mechanical shear forces, and the hydroxyl groups in this HO-G were mainly located at the edges of layer sheets, resulting in the limited content of hydroxyl groups and thus its hydrophilicity is not high enough to obtain a high concentration of the HO-G solution. In the present study, porous thermally reduced graphene oxide could provide more activated carbon atoms, which lead to hydroxyl groups being distributed on the edges of both planar sheets and inner nanopores. Therefore, more hydroxyl groups were introduced onto the basal sheet of graphene, which was favorable to increase the hydrophilicity of HO-G and enhance interfacial interaction between graphene and the C-S-H hydrates.

To examine the surface characteristics of GO, TRGO, and HO-G nanosheets, Fourier transform infrared spectroscopy (FTIR) and X-ray photoelectron spectroscopy (XPS) were conducted. From Figure 1a, the characteristic peaks of GO at 1051, 1223, 1613, 1731, and 3180 cm^{-1} indicated alkoxy C−O stretching, C−OH bending vibrations of hydroxyl groups, C═C skeletal vibration, C═O stretching vibration of carboxyl groups, and the O−H stretching mode, respectively.[28,29] In the FTIR spectrum of TRGO, the absorption peaks at 1573 and 1224 cm^{-1} were related to the skeletal vibration of the aromatic rings and C−OH stretching.[30,31] Compared with the spectrum of GO, the disappearance of the peak at 1731 cm^{-1} indicates the absence of carboxyl groups in TRGO. As for HO-G, the FTIR spectrum demonstrated C−O vibration (1386 and 1077 cm^{-1}) and C═C vibration from sp^2 bonds, but the peak position shifted from 1573 to 1631 cm^{-1} with respect to TRGO. The double absorption bands at 2853 and 2924 cm^{-1} were assigned to C−H groups. A strong signal at 3439 cm^{-1} was detected due to the stretching mode of the hydroxyl group, indicating that the hydroxyl group was successfully grafted into the TRGO backbone. The absorption peak corresponding to C═O stretching of the carboxylic functional group (around 1730 cm^{-1})[31] was not detected, indicating that there was no carboxylic group existing in HO-G. The XPS measurement was undertaken to detect the surface groups of nanosheets. From Figure 1b, the XPS survey spectrum for HO-G (Figure 1b) displayed a C 1s peak at ca. 283.97 eV along with an O 1s peak at ca. 531.97 eV as is the case of GO and TRGO, indicating that there were only C and O elements within HO-G. Figure 1c presents the well-fitted C 1s spectrum of GO, TRGO, and HO-G. In line with the previous study,[28] the result of GO exhibited three peaks at ca. 284.77, 286.87, and 288.62 eV, which correspond to C−C, C−O, and C═O groups, respectively, whereas the C 1s spectrum of TRGO suggested two types of carbon bonds, including the C−C at 284.82 eV and C−O at 286.17 eV.[32] Similarly, there were two peaks at 284.77 and 285.62 eV in the spectrum of HO-G, which could be denoted as C−C and C−O groups, respectively. No signal peaks of carboxyl or carbonyl carbons were detected in the XPS spectrum, which further confirmed hydroxy groups exclusively existing within the HO-G structure. The Raman spectra (Figure 1d) of all of the samples exhibited four main characteristic peaks: the D mode (∼1350 cm^{-1}) produced by the double resonance disorder-induced mode; the G mode (∼1600 cm^{-1}) derived from the in-plane vibration of sp^2 carbon atoms; the symmetry-allowed 2D overtone mode (∼2700 cm^{-1}), and a (D + G) combination pattern (2900 cm^{-1}) induced by the disorder.[32] The peak intensity ratios of the D to G band (I_D/I_G) of GO, TRGO, and HO-G were 0.921, 0.860, and 0.876, respectively. The I_D/I_G of HO-G is slightly higher than that of TRGO, indicating that the sp^3 carbon increased by introducing a number of hydroxyl groups into the graphene lattice and led to the edge distortion and structural defects.[26,33] A solid-state NMR analysis was performed to identify the functional groups of HO-G. As shown in the ^{13}C NMR spectrum of HO-G (Figure S1a), the peaks at 127, 103, 69, and 59 ppm were associated with the sp^2-hybridized carbon, lactol,[34] hydroxyl, and epoxide groups,[35] respectively, while the peaks for the carboxyl and carbonyl carbons were not observed. The ^1H NMR spectrum (Figure S1b) displayed a resonance at ca. 1.9 ppm, corresponding to C−OH.[35,36] Therefore, the NMR analysis strongly suggested that only hydroxyl groups were presented in HO-G.

Figure S2 presents a typical atomic force microscopic (AFM) image of the GO, TRGO, and HO-G obtained from a dilute solution deposited onto a silica mica. The corresponding height profiles of the GO nanosheets (Figure S2b) reveal that the thickness of GO was about 1.9 nm, which composed of 2−3 layers.[37] The AFM image (Figure S2c,d) of TRGO exhibited irregular shapes with a thickness of about 2.4 nm, which corresponded to multilayer graphene (6−7 layers),[38] while the HO-G sheet of the microscale lateral size (∼2 μm) was observed and its thickness was around 1.9 nm (Figure S2e,f), corresponding to three or four graphene layers,[25] indicating that TRGO layers were vigorously exfoliated under mechanical shear forces during the preparation of HO-G. The XRD patterns of GO, TRGO, and HO-G are presented in Figure S3. As shown in the result of GO, a sharp characteristic peak at 12.5° was observed, which was corresponding to the (001) reflection of stacked GO sheets.[23] In contrast to GO, the result of TRGO exhibited a broad diffraction peak (24.9°) and a small diffraction peak (43.3°), which could be attributed to the

https://doi.org/10.1021/acsomega.1c03844
ACS Omega 2021, 6, 30465−30477

(002) and (100) planes of the graphite-like structure.[28] As for the result of HO-G, it presented two characteristic peaks (25.4 and 43.7°) similar to that of TRGO, indicating that the HO-G maintained a typical crystalline structure of graphene. A typical transmission electron microscopic (TEM) image (Figure S4e) shows an almost transparent flake and various wrinkles on the planes of the HO-G sheet, which demonstrated that HO-G had a typical 2D sheet structure, as is the case of GO and TRGO (Figure S4a,c). The high-resolution transmission electron microscopic (HRTEM) image (Figure S4b,d,f) shows that the lattice spacings of GO, TRGO, and HO-G was 0.488, 0.389, and 0.339 nm, respectively, and the lattice spacing of HO-G was in accord with the (002) lattice plane of graphene,[39] indicating that the HO-G maintains a typical crystalline structure of graphene. The selected area electron diffraction (SAED) pattern of HO-G (Figure S5) exhibited a typical diffraction ring of the (002) plane, suggesting that the HO-G presents turbostratic stacking similar to graphene.[23,31] To probe the wettability of HO-G, the HO-G film was prepared to test the contact angle. From Figure S6, the contact angles of GO, HO-G, and TRGO toward water were 23.74, 60.93, and 115.54°, respectively. The excellent hydrophilic nature of GO was mainly attributed to the oxygen-containing groups on its surface, and so it was currently extensively employed to reinforce the cement composites,[4] while poor water wettability was observed for TRGO because most of the functional groups were removed from the surface during the process of thermal reduction of GO.[32] Compared to TRGO, although the wettability of HO-G has been significantly improved because of the introduction of the hydroxyl group, it was worse than that of GO due to the less hydrophilicity of the hydroxyl group than that of the carboxylic group.

2.2. Dispersion Stability of HO-G. *2.2.1. Colloidal Dispersion of Aqueous HO-G Solution.* ζ-Potentials of the aqueous HO-G solution with different concentrations (10, 30, and 50 mg/L) were measured to be ca. −22.7, −27.3, and −33.4 mV (Figure S7a), respectively. The potential value was negative, probably due to the ionization of the phenolic hydroxyl groups on the nanosheet edges and the hydrated shell formed by hydroxyl groups on the basal sheets,[17,40] which indicated the excellent colloidal dispersion of the aqueous HO-G solution. Figure S7b presents the absorbance value of aqueous HO-G solutions (30 mg/L) after 5 min's centrifugation (1000 rpm). No significant loss in absorbance after 5 times of centrifugation indicated the excellent colloidal stability of the HO-G solution. Figure S8 shows the digital photographs of aqueous 30 mg/L HO-G solution kept for 1−30 days. After allowing to stand for 30 days, the homogeneous solution with no obvious aggregations of HO-G was observed, suggesting that HO-G exhibited intrinsically hydrophilic nature and could be very stable in aqueous solution upon exposure to visible light irradiation at ambient temperature for a long time. Several reports showed that visible light irradiation could induce the partial reduction of GO under ambient temperature and thus lead to serious aggregation due to the decreased hydrophilicity of GO.[40,41] Therefore, HO-G was a better choice than GO because its solution was more suitable to stand for long-time for scalable production and engineering applications. Figure S9a shows the UV−vis absorbance spectra for aqueous GO and HO-G solutions. one can easily see that two characteristic peaks were detected in the spectrum of the GO solution. The band located at 230.3 nm was assigned to the $\pi-\pi^*$ plasmon peak from the aromatic C−C bonds in the graphene backbone,[10] and another featured shoulder peak situated at 300.6 nm corresponded to the n−π^* plasmon peak, which was not present in graphene.[42] Obviously, only an absorption peak at 255.4 nm for HO-G dispersions was detected, suggesting the maintenance of the sp^2 conjugated aromatic graphene structure. From Figure S9b, the adsorption intensity of the aqueous HO-G solution at 255.4 nm obeyed the Beer−Lambert law at a HO-G concentration below 30 mg/L,[43] and thus, the absorbance at 255.4 nm was chosen as an indicator to investigate the correlation between the absorbance and the concentration of aqueous HO-G solution.

2.2.2. Dispersion Behavior of Aqueous HO-G Containing Ca^{2+} Ions. Many studies reported that both divalent cations and pH values showed a significant influence on the colloidal dispersion of the GO solution.[8,9] Cation valence such as Ca^{2+} results in the cross-linking of GO nanosheets[44] and a significant reduction of the carboxylic group on the edges of GO at high pH.[7,12] To investigate the effect of Ca^{2+} and the pH value on the colloidal stability of the HO-G solution, the dispersion behavior of HO-G was quantitatively monitored by UV−vis spectroscopy, and the visual observation of sedimentation after standing for different times and the change of the A/A_0 ratio, where the A_0 and A values represented the absorbance of the solution at the initial and different time intervals (t = 10 and 30 min), were calculated to estimate the coagulation degree of HO-G. It was clear that the closer the ratio value to 1, the more stable the solution and thus the less impact of Ca^{2+} and pH on the colloidal stability of the HO-G solution. As shown in Figure 2, the A/A_0 ratios of HO-G in the

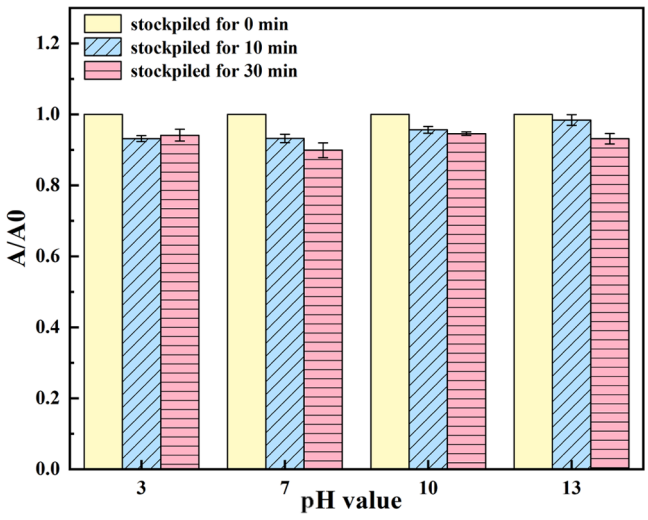

Figure 2. Changes of absorbance of the HO-G solution containing Ca^{2+} at different pH values.

$CaCl_2$ solution (0.1 mol/L, pH = 7) were 0.93 and 0.9 after standing for 10 and 30 min, respectively. The results indicated that the effect of Ca^{2+} on the stability of the HO-G solution was slight, while GO was prone to severely aggregate in a neutral pH environment containing Ca^{2+}.[43] When the pH of the solution increased to 13, the A/A_0 ratios were 0.95 and 0.92 after standing for 10 and 30 min, further implying that the alkaline environment could not induce the reduction of functional groups in HO-G. Moreover, similar phenomena could also be observed when the pH of the solution was adjusted to 3 and 10, respectively. All of these results indicated

https://doi.org/10.1021/acsomega.1c03844
ACS Omega 2021, 6, 30465−30477

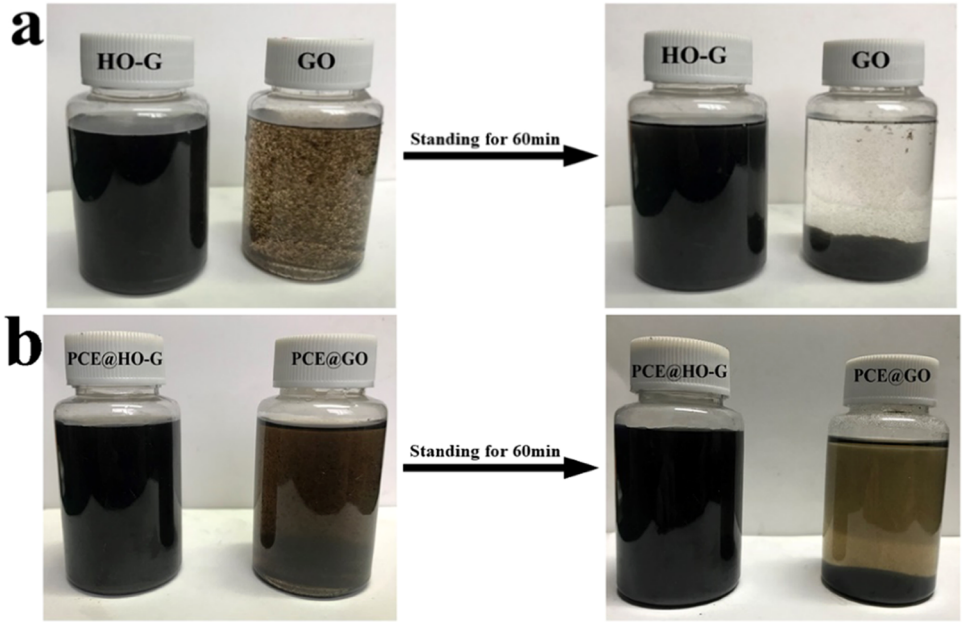

Figure 3. Digital images of (a) HO-G and GO dispersions and (b) polycarboxylate superplasticizer (PCE)@HO-G and PCE@GO suspensions in the saturated $Ca(OH)_2$ solution.

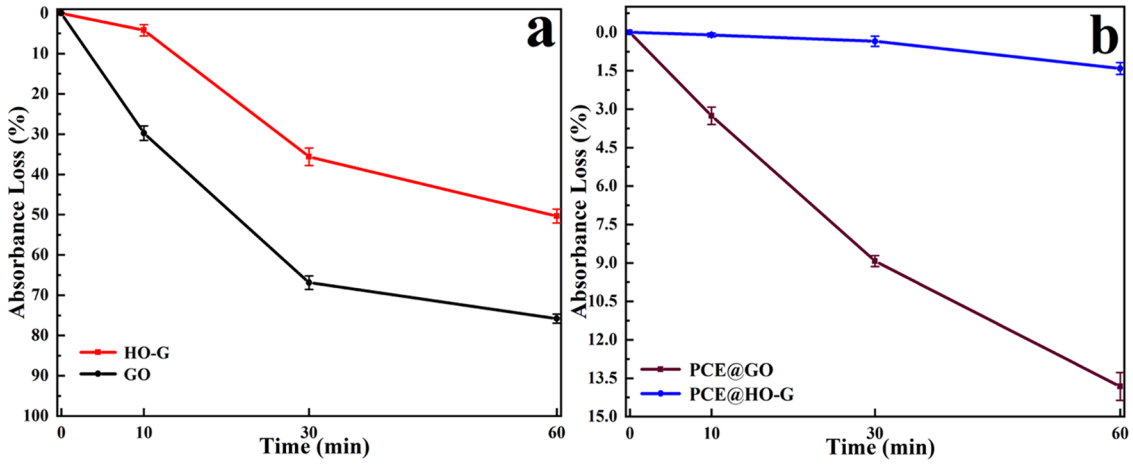

Figure 4. Absorbance loss of (a) HO-G and GO dispersions and (b) PCE@HO-G and PCE@GO suspensions in the saturated $Ca(OH)_2$ solution within 60 min.

the remarkable colloidal stability of aqueous HO-G against Ca^{2+} ions at different pH values.

2.2.3. Dispersion Stability of HO-G in Saturated CH Solution. The dispersion stability of HO-G in the CH solution was studied by the above-mentioned changes of absorbance and visual observation of sedimentation. For comparison, the behavior of GO dispersion was also investigated using the identical procedure. Figure 3a shows the digital images of the dispersion of HO-G and GO in CH solutions. Aggregation of GO occurred immediately when it was introduced into the saturated CH solution, while no obvious change was detected for HO-G. After standing for 60 min, the supernatant solution was almost clear for GO, while no sediments were detected for HO-G. From the absorbance loss curves based on the results of UV−vis for the dispersion of HO-G and GO in the CH solution (Figure 4a), a slight reduction was observed in the absorbance of HO-G after standing for 10 min (nearly 4.1%), while the absorbance of GO reduced sharply (around 29.3%). After standing for 60 min, some degradation in absorbance was exhibited for both GO and HO-G. Compared to that of GO (76.8%), the loss in absorbance of HO-G was 49.2%, which was probably due to the slow reaction of phenolic hydroxyl groups with Ca^{2+}. Therefore, the colloidal stability of the aqueous HO-G solution was less affected by Ca^{2+} in a highly alkaline environment, which was consistent with the results of previous experiments. Moreover, the colloidal dispersion of the HO-G solution was hardly affected by an alkaline cement solution at short intervals (e.g., 10 min) and this was sufficient time for mixing mortar.

Because water-reducer PCE had been proven to have an excellent ability to improve the dispersion of GO in the cement slurry,[10,17] the dispersion behavior of HO-G in the saturated CH solution in the presence of PCE was also investigated. Significantly, no obvious coagulation was observed when PCE was added to GO solutions (Figure 3b). The absorbance losses of GO (Figure 4b) at different standing times (10, 30, and 60 min) were 3.26, 8.93, and 13.82%, respectively. As for HO-G, the absorbance decreased by 0.1, 0.35, and 1.41%, respectively.

https://doi.org/10.1021/acsomega.1c03844
ACS Omega 2021, 6, 30465−30477

These results indicated that the dispersion stability of GO or HO-G in the CH solution could be obviously improved by PCE due to the electrostatic repulsion and steric hindrance.[17,45]

2.3. HO-G Reinforced Cement Mortar. *2.3.1. Effect of HO-G on the Workability of the Cement Mortar.* As shown in Figure 5, the fluidity of the reference sample was 220.5 mm

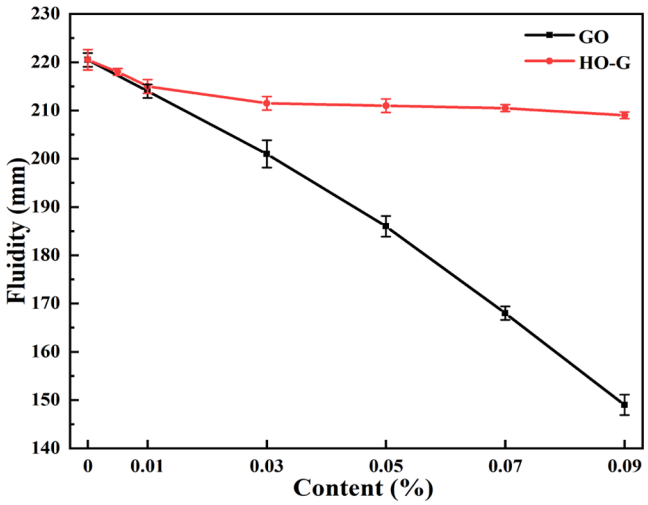

Figure 5. Fluidity of cement mortars with different dosages of GO and HO-G by the cement mass.

and when the contents of GO by the cement weight were 0.01, 0.03, 0.05, 0.07, and 0.09%, the fluidity of $B_{0.01}$, $B_{0.03}$, $B_{0.05}$, $B_{0.07}$, and $B_{0.09}$ was 214, 201, 186, 168, and 149 mm, respectively, suggesting that the fluidity of the cement mortar decreased sharply with the increasing content of GO. This result was consistent with other reports.[18,46] It is widely accepted that the excellent hydrophilicity of GO allowed it to absorb water on its surface, reducing the free water content in the cement system and leading to degrading the fluidity of the cement mortar.[5,46] This has also been validated in the contact angle test for GO (Figure S6). On the other hand, the chemical cross-linking reaction between GO and Ca^{2+} also has a negative influence on the workability of the cement mortar.[11,15] When HO-G was incorporated into the mortar at dosages of 0.005, 0.01, 0.03, 0.05, 0.07, and 0.09% by weight of cement, the fluidity of $C_{0.005}$, $C_{0.01}$, $C_{0.03}$, $C_{0.05}$, $C_{0.07}$, and $C_{0.09}$ was 218, 216, 211.5, 211, 210, and 208 mm, respectively. Only a slight loss of 1.1, 2.0, 4.1, 4.3, 4.8, and 5.7% in the fluidity of the resulting cement mortars were observed compared to that of the reference sample (A_0). This can be explained by the fact that HO-G was less hydrophilic than GO, and thus, its ability to entrap the free water in the fresh slurry was weaker than that of GO, and the lack of active functional groups within HO-G for instant cross-linking reaction with Ca^{2+} could effectively avoid the formation of sediments.

2.3.2. Mechanical Properties. Because HO-G had excellent dispersion stability in the simulated cement pore solution according to the above analysis, it was reasonable to say that HO-G could have a positive effect on the enhanced mechanical properties of cement composites. The effect of HO-G on the mechanical properties of the cement mortar was investigated. For comparison, the mortars containing different GO contents were examined by the identical procedure. From Table 1, the compressive strength was promoted progressively with the increase of the GO content from 0.01 to 0.03 wt % and then decreased with a further increase in the GO dosage from 0.03 to 0.09 wt %. A similar trend was also exhibited in the flexural strength with the increase of the GO content at days 3 and 28. These results indicated that the reinforcement of GO on the cement mortar was closely related to the filler dosage. When the content of GO by the cement mass was 0.03%, the compressive strength of $B_{0.03}$ reached the maximum, which increased by 15.41 and 19.60% compared to the A_0 reference mortar at days 3 and 28, respectively. The maximum enhancements of 3- and 28-day flexural strength were 25 and 18.42% when 0.05 wt % GO was added. This indicated that the addition of a very low dosage of GO could remarkably enhance the mechanical properties of the cement mortar, which was in good agreement with previous reports.[20,45] For the specimens containing HO-G, the enhancement of strength was also highly dependent on the dosage of HO-G in the cement mortar. The compressive strength increased with the increasing HO-G content until the dosage of HO-G reached 0.03 wt %, which reached the maximum value. Compared with the reference mortar, when HO-G was added to the mortar at a content of 0.03% by cement weight, it provided additional 28.62 and

Table 1. Compressive and Flexural Strength of Cement Mortars Containing HO-G or GO at days 3 and 28

	day 3		day 28	
samples	compressive strength[a Mean] (MPa)/change[b] (%)	flexural strength[a Mean] (MPa)/change[b] (%)	compressive strength[a Mean] (MPa)/change[b] (%)	flexural strength[a Mean] (MPa)/change[b] (%)
A_0	31.8 ± 1.3/0	5.2 ± 0.17/0	50.5 ± 0.78/0	11.4 ± 0.22/0
$B_{0.01}$	33.7 ± 1.23/+5.97	5.5 ± 0.26/+5.77	57.9 ± 1.42/+14.65	12.3 ± 0.17/+7.89
$B_{0.03}$	36.7 ± 0.79/+15.41	6.2 ± 0.26/+19.23	60.4 ± 0.75/+19.60	13.4 ± 0.11/+17.54
$B_{0.05}$	33.8 ± 0.36/+6.29	6.5 ± 0.06/+25	58.7 ± 1.06/+16.24	13.5 ± 0.3/+18.42
$B_{0.07}$	31.9 ± 0.82/+0.31	6.1 ± 0.24/+17.31	54.9 ± 0.82/+8.71	12.7 ± 0.35/+11.40
$B_{0.09}$	29.2 ± 1.25/−8.18	5.4 ± 0.17/+3.85	49.9 ± 0.67/−1.18	12.2 ± 0.08/+7.01
$C_{0.005}$	33.9 ± 0.79/+6.6	5.5 ± 0.13/+5.77	56.2 ± 0.52/+11.29	11.9 ± 0.17/+4.39
$C_{0.01}$	36.4 ± 0.44/+14.47	5.4 ± 0.36/+3.85	59.9 ± 0.66/+18.61	12.1 ± 0.25/+6.14
$C_{0.03}$	40.9 ± 1.56/+28.62	5.4 ± 0.2/+3.85	61.2 ± 0.26/+21.19	12.3 ± 0.13/+7.89
$C_{0.05}$	35.8 ± 0.95/+12.58	5.2 ± 0.18/+0	57.9 ± 0.44/+14.65	11.9 ± 0.2/+4.39
$C_{0.07}$	32.6 ± 0.36/+2.52	5.1 ± 0.2/−1.92	52.4 ± 0.72/+3.76	11.7 ± 0.17/+2.63
$C_{0.09}$	32.1 ± 0.82/+0.94	4.8 ± 0.26/−7.69	48.6 ± 0.2/−3.76	11.3 ± 0.2/−0.88

[a Mean]± standard deviation (SD). [b]Compared to A_0.

https://doi.org/10.1021/acsomega.1c03844
ACS Omega 2021, 6, 30465−30477

21.19% enhancements of compressive strength at days 3 and 28, respectively. It is worth noting that the compressive strength of the cement mortar was enhanced greatly at a much lower dosage of HO-G, and a more obvious reinforcement effect of HO-G was exhibited than GO under the same content in the cement mortar. The enhancement in the mechanical performance of a mortar containing HO-G could be attributed to the bridging effect offered by HO-G, which could effectively prevent the formation of microcracks and hinder their extension.[3,47] Moreover, the compressive strength of $B_{0.01}$ increased by 15.41 and 19.60% at 3 and 28 days relative to the A_0 reference mortar. Compared with the mortar containing 0.03 wt % GO, a similar enhancement on the compressive strength of a mortar could be achieved only by the incorporation of 0.01 wt % HO-G. This demonstrated that the reinforcing effect of HO-G as a nanofiller was more outstanding than GO, especially at a low dosage, due to its remarkably homogeneous dispersion in the cement matrix.[48] The lower dosage of HO-G added to cement composites not only exhibited little negative effect on the workability of the fresh cement slurry but also was cost-effective in reinforcing for nanoengineered cement composites. When the HO-G content was further increased to exceed 0.03 wt %, the compressive strength degraded monotonously and consistently. An excessive dosage of HO-G resulted in an adverse impact on the reinforcement of mechanical properties due to the overlapping and aggregation of HO-G together, which was consistent with other reports.[49] As shown in Table 1, the flexural strength of the mortar specimens increased with increasing the content of HO-G from 0.005 to 0.03 wt % and then decreased with the further increase of the HO-G dosage. When 0.03 wt % HO-G was added into the mortar, the flexural strength of $C_{0.03}$ achieved a maximum value with a growth rate of 7.89% at day 28. Due to the adequate interfacial bonding between GO and C-S-H hydrates,[13,15,50] the enhancement efficiency of GO on the flexural strength of the cement mortar was more significant than that of HO-G. Despite this, compared with the same dosage of GO, HO-G exhibited a similar reinforcing effect to cement composites, while only a slightly negative effect on the fresh cement slurry. Meanwhile, for the synthesis of GO, usually the Hummers method was adopted, where flammable and explosive chemicals (such as H_2SO_4, $KMnO_4$) were commonly used, and the purification process was considerably time-consuming.[23,24] On the contrary, the preparation method of HO-G was facile and environmentally friendly. Besides, several nanomaterials have been reported to reinforce the cement composites according to the recent literature surveyed, as shown in Table S1. Compared with the results reported in other studies, it is clear that a very low dosage of HO-G can greatly enhance the mechanical properties of cement composites. As such, HO-G is a promising reinforcing nanofiller for nanoengineered cement composites.

2.3.4. Chloride-Ion Penetration Resistance. Durability is one of the most important properties of cement composites, which is gravely influenced by the transport properties of aggressive agents (e.g., water, chloride, and sulfate).[4,5] In this study, the chloride penetrability of the cement mortar with various HO-G contents was investigated. The chloride penetration depth (X_d) and the non-steady-state migration coefficient D_{RCM} were tested by the rapid chloride migration (RCM) at day 28. As shown in Table 2, the X_d and D_{RCM} of the reference sample were 18.9 mm and 7.3 × 10^{-12} m^2/s, when the contents of HO-G were 0.01, 0.03, 0.05, 0.07, and 0.09 wt %, the X_d and D_{RCM} of the cement mortar were 15.1, 13.5, 13.3, 14.8, and 14.6 mm and 5.7, 5.0, 4.9, 5.7, and 5.6 × 10^{-12} m^2/s, respectively. These results demonstrated that the incorporation of HO-G could remarkably decrease the X_d and D_{RCM} of the cement mortar. When HO-G was added to the mortar at a content of 0.05% by cement weight, the specimen exhibited optimum performance in the reduction of the X_d and D_{RCM} by 29.63 and 32.88% compared to the reference specimen, indicating that the addition of HO-G could effectively block the invasion of chloride by forming a more compacted structure and strong barriers within the cement matrix, which was attributed to the nanofiller effect of nanosheets.[39,49,51,52] This further confirmed the homogeneous dispersion of HO-G in the cement hydration medium.

Table 2. Chloride Migration for Cement Mortars with Different HO-G Contents

	HO-G content[a] (%)	X_d[b,d Mean] (mm)	D_{RCM}[d Mean] (×10^{-12} m^2/s)	change[c] (%)
reference	0	18.9 ± 0.36	7.3 ± 0.2	
HO-G blended cement mortars	0.01	15.1 ± 0.26	5.7 ± 0.24	−21.92
	0.03	13.5 ± 0.78	5.0 ± 0.47	−31.51
	0.05	13.3 ± 0.24	4.9 ± 0.22	−32.88
	0.07	14.8 ± 0.32	5.7 ± 0.17	−21.92
	0.09	14.6 ± 0.44	5.6 ± 0.18	−23.29

[a]Based on the cement weight. [b]X_d represents the chloride penetration depth. [c]Compared to reference. [d Mean]± SD.

2.4. Microstructure of the HO-G-Reinforced Cement Mortar. The capillary pore structure of cement composites plays a decisive role in their mechanical and transport properties.[5,53] To study the effect of HO-G on the pore structure of the mortar, the pore size distribution and porosity for samples A_0 and $C_{0.03}$ were detected by the MIP test at day 28. It is widely accepted that the capillary pores in the cement composites could be divided into large capillaries (50−10 000 nm), mesopores or medium capillaries (10−50 nm), and gel pores (2.5−10 nm).[53,54] The pores with a diameter exceeding 0.05 μm were defined as harmful pores, which corresponded to the critical pore size and were closely related to the mechanical and transport properties (e.g., diffusivity and permeability) of cement composites.[46,55] As shown in Figure 6a, the differential mercury curve of A_0 exhibited multipeaks in the range of 10−10 000 nm, indicating the presence of harmful pores in the reference mortar. In contrast, the curve of $C_{0.03}$ displays a sharp peak at a pore diameter from 0.045 to 0.05 μm and the decreasing of the volume of large capillaries, suggesting that the addition of HO-G could refine the pore structure of the mortar. It could also be further verified from the comparison of the cumulative intrusion curves in Figure 6b. Compared with the reference sample mortar (A_0), the cumulative pore volume curve of $C_{0.03}$ shifted downwards, and the volume of large capillaries in the A_0 specimen (0.0294 mL/g) was higher than that of $C_{0.03}$ (0.0223 mL/g), suggesting that the portion of harmful pores decreased with the addition of HO-G and the pore structure of the hardened mortar has refined. Moreover, the total porosity of $C_{0.03}$ (9.23%) was obviously degraded by 16.12% in comparison to that of A_0 (11.60%). The reduction in the total porosity of $C_{0.03}$ could be due to the nanofiller effect of HO-G, which could fill and divide the large capillaries into finer pores.[2,48] Therefore, the incorporation of HO-G could enhance the compactness of the mortar significantly and

https://doi.org/10.1021/acsomega.1c03844
ACS Omega 2021, 6, 30465−30477

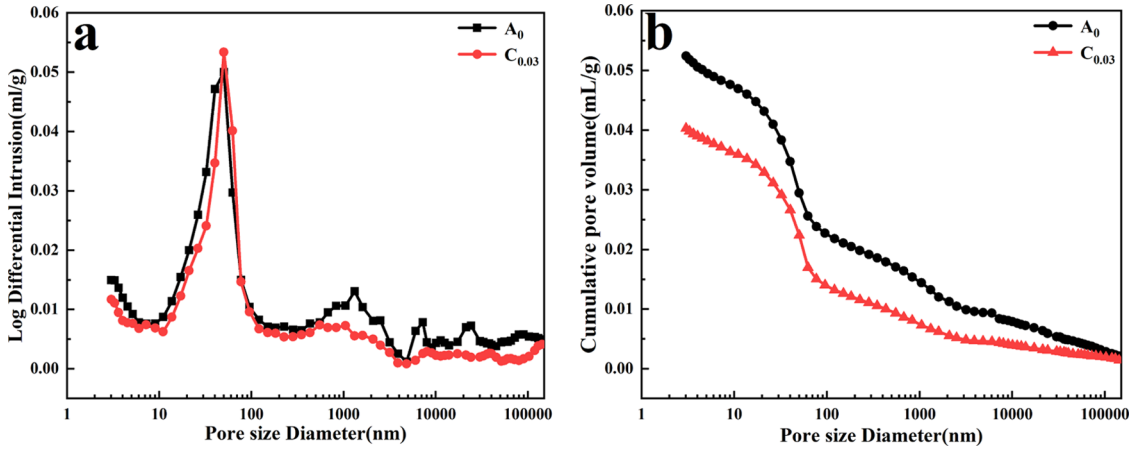

Figure 6. (a) Pore size distribution curves and (b) cumulative pore volume curves of A_0 and $C_{0.03}$.

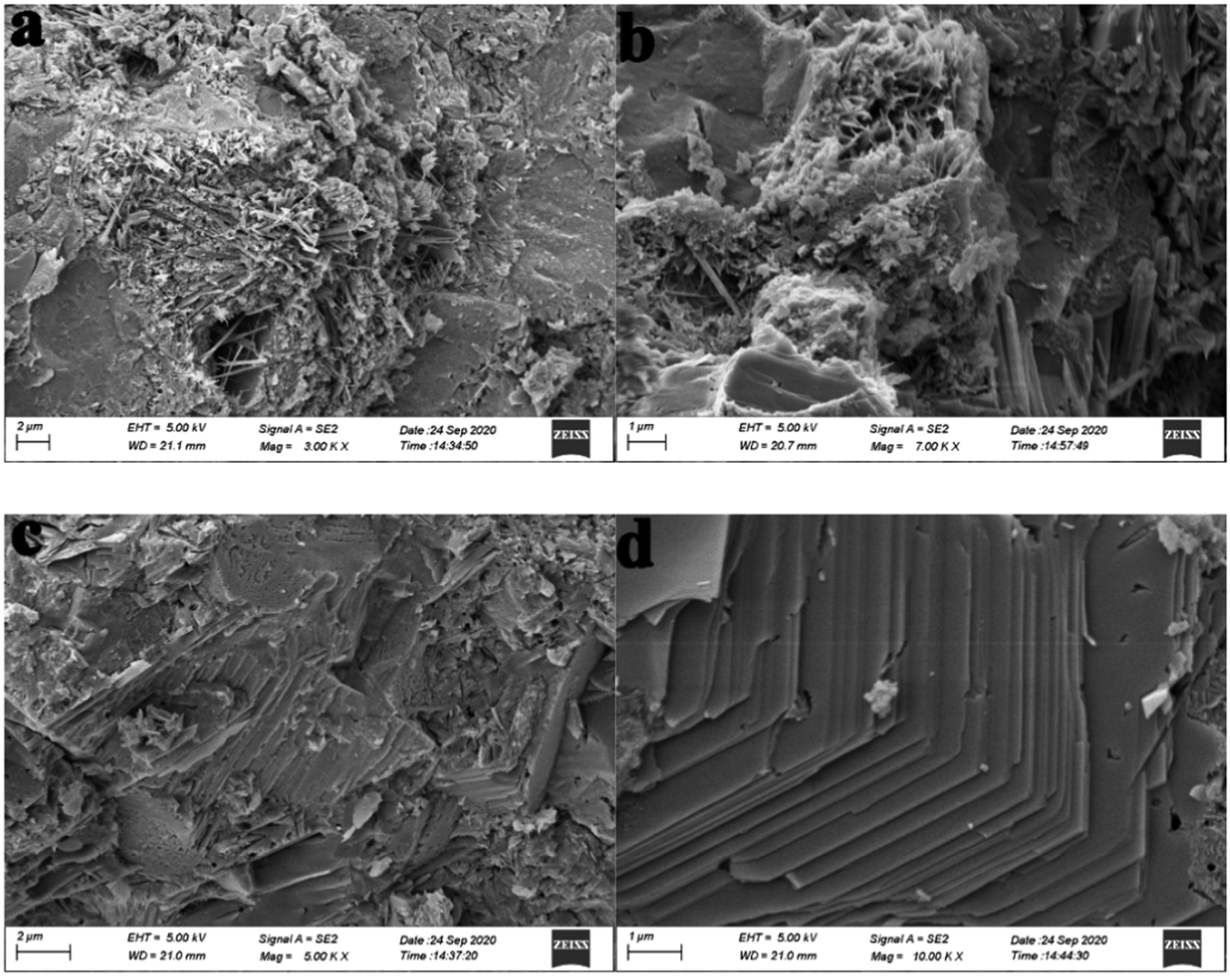

Figure 7. SEM images of mortars A_0 (a, b) and $C_{0.03}$ (c, d) after curing for 28 days.

finally contribute to the improvement in mechanical strength and chloride-ion penetration resistance.

To further investigate the effect of HO-G on the microstructure of the cement mortar, the SEM images of A_0 and $C_{0.03}$ at day 28 were also recorded. From Figure 7a,b of the A_0 sample, some pores, microcrack, and hydration products could be clearly observed and the growth of hydration products interwove with each other, which revealed a disordered, irregular aggregation and a noncompact structure. Compared with A_0, the image of $C_{0.03}$ (Figure 7c) presented a dense structure where no obvious large holes and cracks were observed, indicating that the addition of HO-G could

https://doi.org/10.1021/acsomega.1c03844
ACS Omega 2021, 6, 30465−30477

effectively improve the microstructure and inhibit the crack propagation within the cement mortar by the pore-filling effect and the bridging effect.[5,13,48,56] Figure 7d displayed a regular structure formed by the sheetlike hydration crystals of monosulfates (AFm) or portlandite (CH),[57,58] suggesting that the HO-G also promoted the early cement hydration reaction and produced more hydrated crystals by its nucleation effect.[2,39,52] As discussed above, well-dispersed HO-G in the cement matrix could significantly prevent the formation of microcracks and hinder their extension, refine the pore structure, and favor the growth of hydration products to densify the microstructure of the cement mortar, leading to an improvement in mechanical properties and chloride-ion penetration resistance. Figure S10 presents the XRD spectra of A_0, $C_{0.005}$, $C_{0.01}$, $C_{0.03}$, $C_{0.05}$, $C_{0.07}$, and $C_{0.09}$ at day 28. As shown in the result of A_0, several crystal phases of cement hydration products in the diffraction peaks were observed, which included portlandite (CH) at 18 and 45°; ettringite (AFt) at 34°, 50°, and 68°; tricalcium silicate (C_3S) at 40°; dicalcium silicate (C_2S) at 39°; Calcarea carbonica ($CaCO_3$) at 42°; monosulfates (AFm) at 54 and 68°; and silicon dioxide (SiO_2) at 27 and 36°, respectively. Compared to A_0, there was no obvious shift of these diffraction peaks of hydration products in the HO-G blended cement mortars, except that there were some changes in the intensity of some crystal peaks, indicating that the addition of HO-G hardly affected the type and structure of cement hydration products. With the addition of different contents of HO-G, a clear increase in the intensity of several crystal peaks (such as the CH at 18° and AFm at 54°) was observed, relative to those of the A_0 sample, suggesting that the process of cement hydration was accelerated and more hydration products were produced in the cement system in the presence of HO-G, which was in line with the seeding effects of graphene.[59] In general, the more the hydration products, the more compact the hardened cement mortar.[60] Therefore, it can be concluded that the improvement in mechanical properties and chloride-ion penetration resistance could be attributed to the acceleration of the cement hydration process by HO-G and the formation of more hydration products.

2.5. Hydration Degree. The NEW content of different paste samples at the age of 1, 3, and 28 days was tested to determine the hydration degree of the cement. The NEW content of paste samples after curing for different ages is shown in Figure 8, and obviously, the NEW content was increased with curing age for all of the samples. At 1 day, the NEW content was promoted progressively with the increase of the HO-G content from 0.005 to 0.03 wt %, then decreased with a further increase in the HO-G dosage from 0.03 to 0.09 wt %. When HO-G was added to a mortar at a content of 0.03% by cement mass, the NEW content was increased by 8% compared to that of the reference specimen. This suggested that a certain amount of HO-G could accelerate the hydration process of the cement paste to some degree at the early stage so that more hydration products were formed.[37] After curing for 3 days, the NEW content of the pastes containing HO-G was generally higher than that of the reference samples. With the curing age increased to 28 days, a significant increase in the NEW content of the specimen incorporation of HO-G was observed, and its promotion was more progressive at higher content of HO-G, indicating that the addition of HO-G enhanced the degree of cement hydration, which was in good accordance to the above XRD analysis.

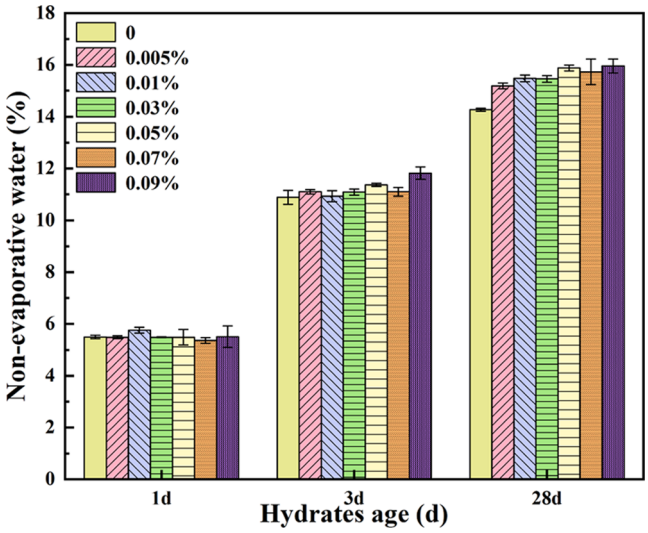

Figure 8. Effect of the HO-G dosage on cement nonevaporative water at different hydrated ages.

3. CONCLUSIONS

Hydroxylated graphene (HO-G) was successfully synthesized by facile one-step solid-state ball milling. Compared to GO, the preparation route of HO-G was more efficient and environmentally friendly and the prepared HO-G nanosheets not only maintained the excellent properties of graphene but also exhibited good hydrophilic nature. Meanwhile, HO-G exhibited considerably superior dispersion stability to GO, whether in water or cement pore solution. The addition of HO-G could remarkably enhance the compressive strength and chloride-ion penetration resistance of the cement mortars. Especially, without an obviously negative effect on the fluidity of the fresh mortar slurry, a similar enhancement in mechanical strength could be achieved even at a much lower dosage of HO-G because it had intrinsic dispersion stability in the cement pore solution. Although the improvement of HO-G on the flexural strength of the mortar was not much pronounced than GO, the real added value in nanoengineering technology was represented by the advancement in the combination properties (e.g., mechanical, workability, durability) of cement composites rather than just the existing mechanical properties. In conclusion, this work not only extends the graphene derivative family but also provides a new solution to develop nanoengineered cement composites.

4. MATERIALS AND METHODS

4.1. Materials. KOH was supplied by Guangdong Guanghua Sci-Tech Co., Ltd. Graphite oxide and GO slurry (the solid content is 43.17%) were provided by The Sixth Element (Changzhou) Materials Technology Co., Ltd. Cement (P.O. 42.5R) was provided from Yonggu New-Type Construction Material Co., Ltd. (Chongqing, China). The chemical composition and physical properties of cement are listed in Tables S2 and S3. The standard sand was purchased from ISO Standard Sand Co., Ltd. (Xiamen, China). The gradation of sand is shown in Table S4. The polycarboxylate superplasticizer (PCE) was provided by Kezhijie New Materials Co., Ltd. (Chongqing, China). The solid content and water-reducing rate of PCE were 50 and 26.7%, respectively.

https://doi.org/10.1021/acsomega.1c03844
ACS Omega 2021, 6, 30465−30477

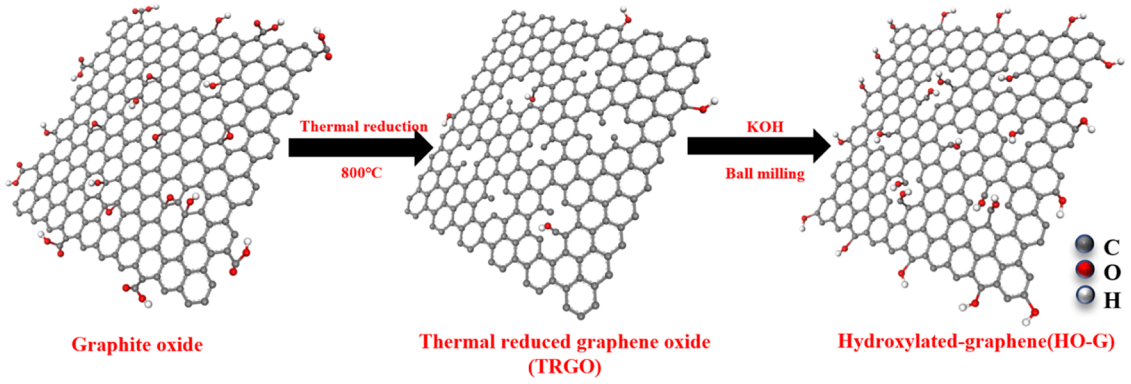

Figure 9. Schematic of the synthesis of HO-G via ball milling.

4.2. Experimental Procedures. *4.2.1. Preparation of HO-G.* To increase the content of hydroxyl groups on the graphene nanosheets, porous thermally reduced graphene oxide (TRGO) was employed as the raw material because many holes and defects were located within the sheets, which provided activated carbon atoms to covalently anchor hydroxyl groups for the solid-state mechanochemical reactions.[61,62] The synthesis process of HO-G was according to our Chinese invention patent (Application No. 202010614203.5). First, TRGO was prepared by the thermal reduction−exfoliation of graphite oxide at 800 °C. Second, TRGO and potassium hydroxide (KOH) were mixed in a mill pot and vigorously shaken by ball milling. Next, the G-OH was obtained by washing and filtering the resulting mixture with the deionized water until the pH was 7. As shown schematically in Figure 9, the nucleophilic attack of hydroxide on the TRGO resulted in the grafting of hydroxyl groups not only on the edge of the TRGO sheet but also bond to the carbon atom located at the edge of in-plane pores during the vigorous balling milling process.

4.2.2. Preparation of Cement Composites Containing HO-G or GO. As an indispensable component in concrete engineering, water-reducer PCE was confirmed to improve the dispersion of GO in the cement alkaline solution.[17,45,63] Before slurry mixing, aqueous HO-G or GO solution was premixed with PCE and then ultrasonicated (UL transonic cleaner CH-06BM, 360W) for 30 min. After that, the nanosheet suspensions were placed in the mixing vessel and then cement was added to the solution and stirred using a JJ-5 type cement mixer (Wuxi Jiangong Test Facility Co. Ltd., China) under a low speed (140 ± 5 rpm) for 30 s; the standard sand was added to the mixture with mixing for 30 s at the same speed and then switched to a high speed (285 ± 10 rpm) for 30 s. Subsequently, the mortar adhering to the bottom and side of the stirring pot was scraped into the mix when stirring was stopped for 90 s. Finally, mixing was carried out for 60 s at a high speed. The water-to-cement ratio of all mixtures was kept constant at 0.36. The mortar preparation method was according to Chinese Standard GB/T 17671-1999, and the mixed proportions of cement mortars are shown in Table S5. GO or HO-G blended mortar composites were named as B_x and C_x (x = 0.005, 0.01, 0.03, 0.05, 0.07, and 0.09), respectively, in which x denoted the weight percentage of GO or HO-G based on the cement mass. After mixing, the fluidity test of the fresh mortar was carried out according to Chinese Standard GB/T 2419-2005. The mixture was loaded into a conical mold (a base diameter of 100 mm, a top diameter of 70 mm, and a height of 60 mm) in two layers. Subsequently, the extra mortar was removed from the top until the cone was leveled. After that, the cone mold was lifted vertically upwards slightly and immediately initiated the jumping table. Then, the diffusion diameters in two mutually perpendicular directions of the mortar were measured by a steel ruler after the table was jerked 25 times. The average value of these two diameters gave the fluidity of the mortar. Then, the mortar was poured into molds and compacted them on a vibration table. The samples were demoulded after 24 h and placed into the curing room (20 °C/RH 90%) until testing. For each mortar mix, three 40 × 40 × 160 mm prisms and three Φ100 × 50 mm discs were prepared. The compressive and flexural strength of the cement mortars were tested at ages of 3 and 28 days. The Φ100 × 50 mm discs were tested for their chloride migration at day 28 according to GB/T 50082-2009.

4.3. Characterization. Fourier transform infrared spectroscopy (FTIR) was performed using a Nicolet iS10 infrared spectrometer (Thermo electron corporation) in the range of 500−4000 cm^{-1}. Solid-state magic angle spinning (MAS) NMR analysis was performed using a Varian VNMR 500 MHz NMR spectrometer. X-ray photoelectron spectroscopy (XPS) measurements were performed on a Thermo Fisher ESCALAB 250Xi photoelectron spectrometer (Waltham, MA) using a monochromatic Al KαX-ray source ($h\nu$ = 1486.6 eV). The thickness of the HO-G sheets was measured using a Bruker's Dimension Icon Atomic force microscope (AFM). A high-resolution transmission electron microscope (HRTEM) was performed using an FEI Tecnai G2 F20 field-emission transmission electron microscope (Hillsboro, OR) at an acceleration voltage of 200 kV. UV−vis spectra were recorded on a TU-1901 UV−vis spectrophotometer. Malvern zetasizer ZEN 3700 was used to measure the ζ-potential of the aqueous colloidal nanosheets. Wettability conductivity was measured with a HARKE-SPACA contact angle meter.

The pore structure of a hardened composite cement mortar was characterized by MIP (MicroActive AutoPore V 9600). After curing for 28 days, the samples were first broken into pieces with a particle size of 1 cm, then soaked in ethanol and stored for at least 24 h to cease further cement hydration. Thereafter, they were dried in a vacuum oven at 80 °C for 24 h. The fracture surfaces of the composites were monitored by a Hitachi SU8020 scanning electron microscopy (SEM). Before the test, the sample was sprayed with gold. The X-ray diffraction (XRD) pattern was recorded on a PANalytical X'pert Pro powder diffractometer (PANalytical. Almelo,

https://doi.org/10.1021/acsomega.1c03844
ACS Omega 2021, 6, 30465−30477

Netherlands) using Cu Kα radiation (λ = 1.5418 Å) with a scan step of 0.013°. Powder samples of an HO-G reinforced cement mortar were produced by grinding at an age of 28 days.

4.4. Dispersion Behavior of the Aqueous HO-G Solution. UV−vis spectroscopy has been widely used to evaluate the dispersion stability of GO in aqueous solution,[43,64] and the dispersion degree of GO in the cement pore solution can be indicated by measuring the absorbance in many studies.[11,43] Therefore, HO-G or GO dispersions (10 mg/L) were first measured by a UV−Vis spectrophotometer in the range of 200−800 nm to detect the maximum wavelength of their solutions and the correlation between the absorbance and the concentration of the aqueous HO-G solution was studied.

It is well known that both Ca^{2+} and pH have a dominant influence on the stability of GO in a cement pore solution.[12] To investigate the dispersion behavior of HO-G in an aqueous solution containing Ca^{2+} ions at different pH values, 5 mL of aqueous HO-G solution (1 mg/mL) was added to 100 mL of $CaCl_2$ solution (0.1 mol/L) and then magnetically stirred for 5 min at 3000 rpm. The coagulation of HO-G induced by Ca^{2+} was quantitatively monitored by the absorbance of the supernatant solution at the maximum wavelength along with visual observation of sedimentation after standing for different times. To investigate the effect of pH on the colloidal dispersion of aqueous HO-G containing Ca^{2+} ions, 10 mmol/L HCl or NaOH was added to the solution until the pH values were 3, 10, and 13, respectively.

4.5. Dispersion of HO-G in a Simulated Alkaline Cement Pore Solution. It has been universally acknowledged that the effectiveness of nanosheets in enhancing the performance of cement composites should be closely related to its well dispersion in the cement hydration medium.[39,50] To further investigate the dispersion stability of HO-G in the alkaline cement slurry, a saturated $Ca(OH)_2$ solution (CH) was chosen to simulate the cement pore solution, which was also frequently used in other studies.[11,43,45,64] First, 5 mL of HO-G or GO aqueous solution (1 mg/mL) was added to 100 mL of saturated CH solution. After being magnetically stirred for 5 min, the aggregation behaviors of GO and HO-G were visually observed, and the supernatant absorbance at a maximum wavelength was also tested as an indicator to show the stability of HO-G or GO colloidal dispersion against different standing times in the presence of CH.

Considering that water-reducer PCE is an indispensable component in concrete engineering,[45] the dispersion behavior of HO-G nanosheets in saturated CH solution in the presence of PCE was also investigated. Then, 20 mL of aqueous HO-G or GO solution (0.2 mg/mL) was premixed with 0.5 mL of water-reducer PCE and ultrasonicated (UL transonic cleaner CH-06BM, 360W) for 30 min. Then, two different suspensions (labeled as PCE@GO, PCE@HO-G) were added into 100 mL of saturated CH solution and stirred for 5 min. Finally, the coagulation behaviors of two colloidal solutions were detected by the change of absorbance at different time intervals.

4.6. Hydration Degree. To determine the effect of HO-G on the hydration process of the cement composites, the nonevaporative water (NEW) content was tested to characterize the hydration degree of hardened cement pastes.[65] HO-G was added into the cement paste at six different contents (0.005, 0.01, 0.03, 0.05, 0.07, and 0.09%) by the cement weight, and the plain cement paste without HO-G served as the reference sample. After curing for different ages, the samples were soaked in ethyl alcohol for 24 h and then ground to powder until it was passed through an 80 μm sieve and then predried at 65 °C in a vacuum oven until the weight remained unchanged. Approximately 1−2 g of dried sample powder was dehydrated at 1000 °C for 3 h. The NEW content was calculated by the following formula (1)[37]

$$\mathrm{CW} = \frac{(100 - L)m_1 - 100m_2}{m_2} \quad (1)$$

where CW is the NEW content (%), L is the cement loss of ignition (1.25), m_1 is the weight of the sample before testing (g), m_2 is the weight of the sample after testing (g).

■ ASSOCIATED CONTENT

Supporting Information

The Supporting Information is available free of charge at https://pubs.acs.org/doi/10.1021/acsomega.1c03844.

Characterization of the nanomaterials employed in the present work by NMR, AFM, TEM, XRD, UV−vis analysis, and the contact angle test; colloidal dispersion of aqueous HO-G solution; chemical compositions and physical properties of cement; gradation of standard sand; mix proportion of cement mortars; and comparisons of HO-G against other nanofillers for the enhancement of cement composites (PDF)

■ AUTHOR INFORMATION

Corresponding Author

Xiaoya Yuan − *College of Materials Science and Engineering, Chongqing Jiaotong University, Chongqing 400074, China;* orcid.org/0000-0002-0942-4366; Phone: +86-23-62789154; Email: yuanxy@cqjtu.edu.cn.

Authors

Sen Yang − *College of Materials Science and Engineering, Chongqing Jiaotong University, Chongqing 400074, China*

Wen Jia − *College of Materials Science and Engineering, Chongqing Jiaotong University, Chongqing 400074, China*

Yuangui Wang − *College of Materials Science and Engineering, Chongqing Jiaotong University, Chongqing 400074, China*

Weifu Zhang − *College of Materials Science and Engineering, Chongqing Jiaotong University, Chongqing 400074, China*

Complete contact information is available at: https://pubs.acs.org/10.1021/acsomega.1c03844

Notes

The authors declare no competing financial interest.

■ ACKNOWLEDGMENTS

The authors would like to gratefully acknowledge financial support from the National Natural Science Foundation of China (no. 51402030), the Natural Science Foundation of the Chongqing Science and Technology Commission (cstc2017jcyjBX0028), and the Science and Technology Research Program of Chongqing Municipal Education Commission (KJZD-K201800703).

■ REFERENCES

(1) Zhao, Z.; Qi, T.; Zhou, W.; Hui, D.; Xiao, C.; Qi, J.; Zheng, Z.; Zhao, Z. A review on the properties, reinforcing effects, and commercialization of nanomaterials for cement-based materials. *Nanotechnol. Rev.* **2020**, *9*, 303−322.

(2) Lin, Y.; Du, H. Graphene reinforced cement composites: A review. *Constr. Build. Mater.* **2020**, *265*, No. 120312.
(3) Du, H.; Pang, S. D. Dispersion and stability of graphene nanoplatelet in water and its influence on cement composites. *Constr. Build. Mater.* **2018**, *167*, 403−413.
(4) Xu, Y.; Zeng, J.; Chen, W.; Jin, R.; Li, B.; Pan, Z. A holistic review of cement composites reinforced with graphene oxide. *Constr. Build. Mater.* **2018**, *171*, 291−302.
(5) Zhao, L.; Guo, X.; Song, L.; Song, Y.; Dai, G.; Liu, J. An intensive review on the role of graphene oxide in cement-based materials. *Constr. Build. Mater.* **2020**, *241*, No. 117939.
(6) Tang, H.; Zhang, S.; Huang, T.; Cui, F.; Xing, B. Effects of pH and electrolytes on the sheet-to-sheet aggregation mode of graphene oxide in aqueous solutions. *Environ. Sci.: Nano* **2020**, *7*, 984−995.
(7) Chowdhury, I.; Mansukhani, N. D.; Guiney, L. M.; Hersam, M. C.; Bouchard, D. Aggregation and Stability of Reduced Graphene Oxide: Complex Roles of Divalent Cations, pH, and Natural Organic Matter. *Environ. Sci. Technol.* **2015**, *49*, 10886−10893.
(8) Chowdhury, I.; Duch, M. C.; Mansukhani, N. D.; Hersam, M. C.; Bouchard, D. Colloidal Properties and Stability of Graphene Oxide Nanomaterials in the Aquatic Environment. *Environ. Sci. Technol.* **2013**, *47*, 6288−6296.
(9) Wu, L.; Liu, L.; Gao, B.; Muñoz-Carpena, R.; Zhang, M.; Chen, H.; Zhou, Z.; Wang, H. Aggregation Kinetics of Graphene Oxides in Aqueous Solutions: Experiments, Mechanisms, and Modeling. *Langmuir* **2013**, *29*, 15174−15181.
(10) Chuah, S.; Li, W.; Chen, S. J.; Sanjayan, J. G.; Duan, W. H. Investigation on dispersion of graphene oxide in cement composite using different surfactant treatments. *Constr. Build. Mater.* **2018**, *161*, 519−527.
(11) Li, X.; Korayem, A. H.; Li, C.; Liu, Y.; He, H.; Sanjayan, J. G.; Duan, W. H. Incorporation of graphene oxide and silica fume into cement paste: A study of dispersion and compressive strength. *Constr. Build. Mater.* **2016**, *123*, 327−335.
(12) Ghazizadeh, S.; Duffour, P.; Skipper, N. T.; Billing, M.; Bai, Y. An investigation into the colloidal stability of graphene oxide nanolayers in alite paste. *Cem. Concr. Res.* **2017**, *99*, 116−128.
(13) Wang, M.; Wang, R.; Yao, H.; Farhan, S.; Zheng, S.; Du, C. Study on the three dimensional mechanism of graphene oxide nanosheets modified cement. *Constr. Build. Mater.* **2016**, *126*, 730−739.
(14) Yuan, X.; Niu, J.; Zeng, J.; Jing, Q. Cement-Induced Coagulation of Aqueous Graphene Oxide with Ultrahigh Capacity and High Rate Behavior. *Nanomaterials* **2018**, *8*, No. 574.
(15) Kai, M. F.; Zhang, L. W.; Liew, K. M. Graphene and graphene oxide in calcium silicate hydrates: Chemical reactions, mechanical behavior and interfacial sliding. *Carbon* **2019**, *146*, 181−193.
(16) Korayem, A. H.; Tourani, N.; Zakertabrizi, M.; Sabziparvar, A. M.; Duan, W. H. A review of dispersion of nanoparticles in cementitious matrices: Nanoparticle geometry perspective. *Constr. Build. Mater.* **2017**, *153*, 346−357.
(17) Zhao, L.; Guo, X.; Liu, Y.; Ge, C.; Chen, Z.; Guo, L.; Shu, X.; Liu, J. Investigation of dispersion behavior of GO modified by different water reducing agents in cement pore solution. *Carbon* **2018**, *127*, 255−269.
(18) Shang, Y.; Zhang, D.; Yang, C.; Liu, Y.; Liu, Y. Effect of graphene oxide on the rheological properties of cement pastes. *Constr. Build. Mater.* **2015**, *96*, 20−28.
(19) Wang, M.; Yao, H.; Wang, R.; Zheng, S. Chemically functionalized graphene oxide as the additive for cement−matrix composite with enhanced fluidity and toughness. *Constr. Build. Mater.* **2017**, *150*, 150−156.
(20) Kang, D.; Seo, K. S.; Lee, H.; Chung, W. Experimental study on mechanical strength of GO-cement composites. *Constr. Build. Mater.* **2017**, *131*, 303−308.
(21) Abrishami, M. E.; Zahabi, V. Reinforcing graphene oxide/cement composite with NH2 functionalizing group. *Bull. Mater. Sci.* **2016**, *39*, 1073−1078.
(22) Lu, L.; Zhao, P.; Lu, Z. A short discussion on how to effectively use graphene oxide to reinforce cementitious composites. *Constr. Build. Mater.* **2018**, *189*, 33−41.
(23) Alam, S. N.; Sharma, N.; Kumar, L. Synthesis of Graphene Oxide (GO) by Modified Hummers Method and Its Thermal Reduction to Obtain Reduced Graphene Oxide (rGO)*. *Graphene* **2017**, *6*, 1−18.
(24) Zaaba, N. I.; Foo, K. L.; Hashim, U.; Tan, S. J.; Voon, C. H.; et al. Synthesis of Graphene Oxide using Modified Hummers Method: Solvent Influence. *Procedia Eng.* **2017**, *184*, 469−477.
(25) Sun, J.; Deng, Y.; Li, J.; Wang, G.; He, P.; Tian, S.; Bu, X.; Di, Z.; Yang, S.; Ding, G.; Xie, X. A New Graphene Derivative: Hydroxylated Graphene with Excellent Biocompatibility. *ACS Appl. Mater. Interfaces* **2016**, *8*, 10226−10233.
(26) Yan, L.; Lin, M.; Zeng, C.; Chen, Z.; Liu, Y.; et al. Electroactive and biocompatible hydroxyl- functionalized graphene by ball milling. *J. Mater. Chem.* **2012**, *22*, 8367−8371.
(27) Majumdar, D.; Bhattacharya, S. K. Sonochemically synthesized hydroxy-functionalized graphene−MnO2 nanocomposite for supercapacitor applications. *J. Appl. Electrochem.* **2017**, *47*, 789−801.
(28) Alkhouzaam, A.; Qiblawey, H.; Khraisheh, M.; Atieh, M.; Al-Ghouti, M. Synthesis of graphene oxides particle of high oxidation degree using a modified Hummers method. *Ceram. Int.* **2020**, *46*, 23997−24007.
(29) Lv, S.; Hu, H.; Hou, Y.; Lei, Y.; Sun, L.; Zhang, J.; Liu, L. Investigation of the Effects of Polymer Dispersants on Dispersion of GO Nanosheets in Cement Composites and Relative Microstructures/Performances. *Nanomaterials* **2018**, *8*, No. 964.
(30) Raza, M. A.; Maqsood, M. F.; Rehman, Z. U.; Westwood, A.; Inam, A.; Sattar, M. M. S.; Ghauri, F. A.; Ilyas, M. T. Thermally Reduced Graphene Oxide-Reinforced Acrylonitrile Butadiene Styrene Composites Developed by Combined Solution and Melt Mixing Method. *Arabian J. Sci. Eng.* **2020**, *45*, 9559−9568.
(31) Luo, Z.; Li, Y.; Wang, F.; Hong, R. Plasma Exfoliated Graphene: Preparation via Rapid, Mild Thermal Reduction of Graphene Oxide and Application in Lithium Batteries. *Materials* **2019**, *12*, No. 707.
(32) Dao, T. D.; Jeong, H. M. Graphene prepared by thermal reduction−exfoliation of graphite oxide: Effect of raw graphite particle size on the properties of graphite oxide and graphene. *Mater. Res. Bull.* **2015**, *70*, 651−657.
(33) López-Díaz, D.; Delgado-Notario, J. A.; Clericò, V.; Diez, E.; Velázquez, M. Towards Understanding the Raman Spectrum of Graphene Oxide: The Effect of the Chemical Composition. *Coatings* **2020**, *10*, No. 524.
(34) Xue, H.; Lu, Y.; Geng, H.; Dong, B.; Wu, S.; Fan, Q.; Zhang, Z.; Li, X.; Zhou, X.; Wang, J. Hydroxyl Groups on the Graphene Surfaces Facilitate Ice Nucleation. *J. Phys. Chem. Lett.* **2019**, *10*, 2458−2462.
(35) Vacchi, I. A.; Spinato, C.; Raya, J.; Bianco, A.; Menard-Moyon, C. Chemical reactivity of graphene oxide towards amines elucidated by solid-state NMR. *Nanoscale* **2016**, *8*, 13714−13721.
(36) Panich, A. M.; Shames, A. I.; Sergeev, N. A. Paramagnetic Impurities in Graphene Oxide. *Appl. Magn. Reson.* **2013**, *44*, 107−116.
(37) Wei, Z.; Wang, Y.; Qi, M.; Bi, J.; Yang, S.; Yuan, X. The role of sucrose on enhancing properties of graphene oxide reinforced cement composites containing fly ash. *Constr. Build. Mater.* **2021**, *293*, No. 123507.
(38) Gurzęda, B.; Florczak, P.; Wiesner, M.; Kempiński, M.; Jurga, S.; Krawczyk, P. Graphene material prepared by thermal reduction of the electrochemically synthesized graphite oxide. *RSC Adv.* **2016**, *6*, 63058−63063.
(39) Yang, H.; Cui, H.; Tang, W.; Li, Z.; Han, N.; Xing, F. A critical review on research progress of graphene/cement based composites. *Composites, Part A* **2017**, *102*, 273−296.
(40) Gao, Y.; Ren, X.; Song, G.; Chen, D.; Zhang, X.; Chen, C. Colloidal properties and stability of UV-transformed graphene oxide in aqueous solutions: The role of disorder degree. *J. Hazard. Mater.* **2020**, *382*, No. 121097.

https://doi.org/10.1021/acsomega.1c03844
ACS Omega 2021, 6, 30465−30477

(41) Chowdhury, I.; Hou, W. C.; Goodwin, D.; Henderson, M.; Zepp, R. G.; Bouchard, D. Sunlight affects aggregation and deposition of graphene oxide in the aquatic environment. *Water Res.* **2015**, *78*, 37−46.
(42) Li, W.; Li, X.; Chen, S. J.; Liu, Y. M.; Duan, W. H.; Shah, S. P. Effects of graphene oxide on early-age hydration and electrical resistivity of Portland cement paste. *Constr. Build. Mater.* **2017**, *136*, 506−514.
(43) Lin, J.; Shamsaei, E.; Basquiroto de Souza, F.; Sagoe-Crentsil, K.; Duan, W. H. Dispersion of graphene oxide−silica nanohybrids in alkaline environment for improving ordinary Portland cement composites. *Cem. Concr. Compos.* **2020**, *106*, No. 103488.
(44) Yang, K.; Chen, B.; Zhu, X.; Xing, B. Aggregation, Adsorption, and Morphological Transformation of Graphene Oxide in Aqueous Solutions Containing Different Metal Cations. *Environ. Sci. Technol.* **2016**, *50*, 11066−11075.
(45) Zhao, L.; Guo, X.; Ge, C.; Li, Q.; Guo, L.; Shu, X.; Liu, J. Mechanical behavior and toughening mechanism of polycarboxylate superplasticizer modified graphene oxide reinforced cement composites. *Composites, Part B* **2017**, *113*, 308−316.
(46) Li, X.; Liu, Y. M.; Li, W. G.; Li, C. Y.; Sanjayan, J. G.; Duan, W. H.; Li, Z. Effects of graphene oxide agglomerates on workability, hydration, microstructure and compressive strength of cement paste. *Constr. Build. Mater.* **2017**, *145*, 402−410.
(47) Ho, V. D.; Ng, C.-T.; Coghlan, C. J.; Goodwin, A.; Mc Guckin, C.; Ozbakkaloglu, T.; Losic, D. Electrochemically produced graphene with ultra large particles enhances mechanical properties of Portland cement mortar. *Constr. Build. Mater.* **2020**, *234*, No. 117403.
(48) Krystek, M.; Pakulski, D.; Patroniak, V.; Górski, M.; Szojda, L.; Ciesielski, A.; Samorì, P. High-Performance Graphene-Based Cementitious Composites. *Adv. Sci.* **2019**, *6*, No. 1801195.
(49) Li, G.; Yuan, J. B.; Zhang, Y. H.; Zhang, N.; Liew, K. M. Microstructure and mechanical performance of graphene reinforced cementitious composites. *Composites, Part A* **2018**, *114*, 188−195.
(50) Jing, G.; Feng, H.; Li, Q.; Li, X.; Wu, J.; Wang, S.; Cheng, X.; Ye, Z. Enhanced Dispersion of Graphene Oxide in Cement Matrix with Isolated-Dispersion Strategy. *Ind. Eng. Chem. Res.* **2020**, *59*, 10221−10228.
(51) Mohammed, A.; Sanjayan, J. G.; Duan, W. H.; Nazari, A. Incorporating graphene oxide in cement composites: A study of transport properties. *Constr. Build. Mater.* **2015**, *84*, 341−347.
(52) Du, H.; Gao, H. J.; Pang, S. D. Improvement in concrete resistance against water and chloride ingress by adding graphene nanoplatelet. *Cem. Concr. Res.* **2016**, *83*, 114−123.
(53) Zhao, L.; Guo, X.; Liu, Y.; Zhao, Y.; Chen, Z.; Zhang, Y.; Guo, L.; Shu, X.; Liu, J. Hydration kinetics, pore structure, 3D network calcium silicate hydrate, and mechanical behavior of graphene oxide reinforced cement composites. *Constr. Build. Mater.* **2018**, *190*, 150−163.
(54) Bai, S.; Jiang, L.; Xu, N.; Jin, M.; Jiang, S. Enhancement of mechanical and electrical properties of graphene/cement composite due to improved dispersion of graphene by addition of silica fume. *Constr. Build. Mater.* **2018**, *164*, 433−441.
(55) Jin, M.; Jiang, L.; Zhu, Q. Monitoring chloride ion penetration in concrete with different mineral admixtures based on embedded chloride ion selective electrodes. *Constr. Build. Mater.* **2017**, *143*, 1−15.
(56) Kang, X.; Zhu, X.; Qian, J.; Liu, J.; Huang, Y. Effect of graphene oxide (GO) on hydration of tricalcium silicate (C3S). *Constr. Build. Mater.* **2019**, *203*, 514−524.
(57) Baomin, W.; Shuang, D. Effect and mechanism of graphene nanoplatelets on hydration reaction, mechanical properties and microstructure of cement composites. *Constr. Build. Mater.* **2019**, *228*, No. 116720.
(58) Wang, B.; Shuang, D. Effect of graphene nanoplatelets on the properties, pore structure and microstructure of cement composites. *Mater. Express* **2018**, *8*, 407−416.
(59) Birenboim, M.; Nadiv, R.; Alatawna, A.; Buzaglo, M.; Schahar, G.; Lee, J.; Kim, G.; Peled, A.; Regev, O. Reinforcement and workability aspects of graphene-oxide-reinforced cement nanocomposites. *Composites, Part B* **2019**, *161*, 68−76.
(60) Liu, J.; Fu, J.; Yang, Y.; Gu, C. Study on dispersion, mechanical and microstructure properties of cement paste incorporating graphene sheets. *Constr. Build. Mater.* **2019**, *199*, 1−11.
(61) Farah, S.; Farkas, A.; Madarász, J.; László, K. Comparison of thermally and chemically reduced graphene oxides by thermal analysis and Raman spectroscopy. *J. Therm. Anal. Calorim.* **2020**, *142*, 331−337.
(62) Zhang, X.; Han, S.; Xiao, P.; Fan, C.; Zhang, W. Thermal reduction of graphene oxide mixed with hard carbon and their high performance as lithium ion battery anode. *Carbon* **2016**, *100*, 600−607.
(63) Wang, Q.; Li, S.-y.; Pan, S.; Guo, Z.-w. Synthesis and properties of a silane and copolymer-modified graphene oxide for use as a water-reducing agent in cement pastes. *New Carbon Mater.* **2018**, *33*, 131−139.
(64) Yang, H.; Monasterio, M.; Cui, H.; Han, N. Experimental study of the effects of graphene oxide on microstructure and properties of cement paste composite. *Composites, Part A* **2017**, *102*, 263−272.
(65) Kong, X.-M.; Liu, H.; Lu, Z.-B.; Wang, D.-M. The influence of silanes on hydration and strength development of cementitious systems. *Cem. Concr. Res.* **2015**, *67*, 168−178.

https://doi.org/10.1021/acsomega.1c03844
ACS Omega 2021, 6, 30465−30477